ELSEVIER

J. Non-Newtonian Fluid Mech. 119 (2004) 61–69

Journal of Non-Newtonian Fluid Mechanics

www.elsevier.com/locate/jnnfm

Electrohydrodyamic convection in small aspect ratio devices

T. Mullin [a,*], S.J. Tavener [b], G.I. Blake [a]

[a] *Department of Physics and Astronomy, University of Manchester, Manchester M13 9PL, UK*
[b] *Department of Mathematics, Colorado State University, Fort Collins, CO 80523, USA*

Received 16 January 2002; received in revised form 1 August 2002

This article is part of a Special Issue dedicated to the memory of Frank Leslie

Abstract

We present numerical and experimental results on steady electrohydrodynamic convection in nematic liquid crystal flows. Numerical bifurcation techniques have been applied to the Ericksen–Leslie equations in finite two-dimensional domains in order to investigate the interaction between neighbouring instabilities. A cusp has been uncovered in the solution surface in qualitative agreement with complimentary experiments.

Keywords: Electrohydrodyamic convection; Cellular exchange; Rusp

1. Introduction

When an electric field is applied across a thin layer of nematic liquid crystal, a hydrodynamic instability in the form of a set of rolls can occur above a critical field strength. The length and velocity scales involved in these microscopic flows are small so that the conventional Reynolds number is very much less than one. The nonlinearity which gives rise to the instability originates in the material properties. Details of the mechanisms involved are complex but well-understood and a brief review of them will be presented below. In common with other hydrodynamic instability problems, a significant amount of progress has been made through a combination of theoretical and experimental research. Both one and two-dimensional analyses of the linearized equations of motion have been performed and good agreement between observation and calculation has been achieved. A modern account of this research can be found in [9].

Nematic liquid crystals differ from normal isotropic fluids since they exhibit long–range orientational ordering. They flow readily since the usual viscosity is comparable with that of normal fluids such as water. However, they contain rod-like molecules which are arranged, on average, with their long axes parallel to one another. Hence their friction coefficients are anisotropic and these can be modelled by various viscosities commonly called Leslie coefficients. In addition, the centres of mass of the molecules are randomly distributed so that they only have one preferred spatial orientation. The direction of alignment is described by the unit vector $\boldsymbol{n}$ which is called the director. In practical devices the orientation is provided by surface treatments which are mechanical in nature as discussed by [3]. This local arrangement of the molecules by the boundaries in turn influences the bulk fluid and since most practical situations are concerned with length scales of tens of microns, good alignment can be achieved. The interested reader is referred to [7,11,16] for a discussion of the rich properties of nematic and other liquid crystals.

The microscopic molecular alignment of nematics means that they have anisotropic macroscopic properties. They are optically and dielectrically anisotropic and it is the former property which makes them so useful in display devices. The dielectric anisotropy is $\Delta\epsilon = \epsilon_{\parallel} - \epsilon_{\perp}$, where the symbols $\parallel$ and $\perp$ refer to directions parallel and perpendicular to $\boldsymbol{n}$. This quantity may be either positive or negative and electrohydrodynamic convection is usually found when this quantity is negative or slightly positive. If the material has a strongly positive dielectric anisotropy then a static realigment instability under the application of a perpendicular magnetic or electric field is found. This is called the Freedericksz transition and has been investigated recently using numerical bifurcation techniques by [6]. In practice, most nematic materials contain some free ions so that they are weakly conducting and the anisotropic conductivity is given

* Corresponding author.
E-mail address: tom@reynolds.ph.man.ac.uk (T. Mullin).

0377-0257/$ – see front matter
doi:10.1016/j.jnnfm.2002.08.001

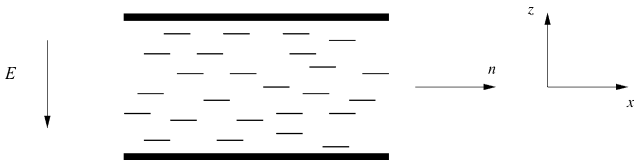

Fig. 1. Schematic of experiment.

by $\Delta\sigma = \sigma_{\parallel} - \sigma_{\perp}$. This is positive in most materials so that conduction along the direction of the molecules is preferred.

The continuum equations of motion for a nematic are the Ericksen–Leslie equations and all the existing evidence suggests that they provide a good model of the flow properties. In order to examine flows in domains of finite size, we solve the Ericksen–Leslie equations and their boundary conditions directly using the finite-element method. Finite size effects are of great practical significance since many modern devices using these materials are becoming smaller and there is a need for a detailed understanding of flow properties. The multiplicity of the solution set is reduced in microscopic devices allowing the detailed investigation of individual dynamical events which lead to low-dimensional chaos (see [5,24,25,27,28,37]). Hence, there is also a need here for calculations of flows in finite domains.

An alternative approach to the study of electrohydrodynamic convection, in the spirit of [15], involves the construction of expansions about the basic state leading to the development of a (generalized) Ginzburg–Landau equation to approximate weakly nonlinear phenomena. This approach, including an extended weak electrolyte model developed to provide a basis for understanding the Hopf bifurcation that can be observed at threshold in certain regions of parameter space and the effect of thermal noise, has been extensively reviewed elsewhere by [9,31,40].

1.1. Electrohydrodynamic convection

The electrohydrodynamic instability can be understood as follows. Consider a nematic liquid crystal material, with planar alignment, contained between two conducting plates as shown schematically in Fig. 1. An electric field is applied vertically and for materials with negative dielectric anisotropy this provides a stabilising force. Suppose now that the field is increased and consider a small horizontally periodic perturbation to the director field. Charge separation will occur due to the conductivity anisotropy and space charges will build up preferentially in the regions of strongest curvature of the director. For an applied field directed vertically downwards, this charge concentration will be positive where the curvature is convex and negative where it is concave. The interaction of the nonuniform space charge distribution with the applied electric field will produce material flow in opposite vertical directions. This results in an additional shear on the molecules which will increase the curvature. Hence an instability can develop in the form of a series of parallel rolls which rotate in opposite directions as shown in Fig. 2.

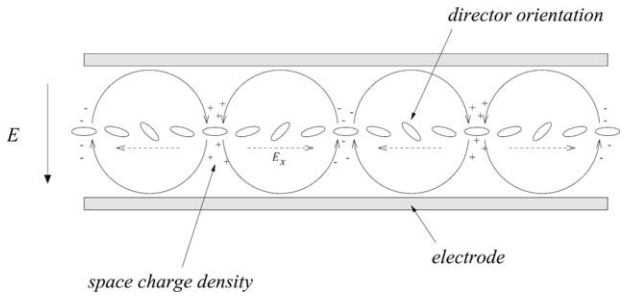

Fig. 2. Instability mechanism.

The angular displacement of the directors will be opposed by the elastic forces induced by the wall alignment and by the negative dielectric anisotropy since the molecules prefer to remain orthogonal to the local electric field. Fluid motions will of course be opposed by the presence of the nearby conducting plates on which non-slip boundary conditions pertain and eventually a balance will be achieved. By way of analogy with Bénard convection, where heat is transported from the hot wall to the cold one by convection, here the motion acts to redistribute the charges between the positive and negative regions which are periodically displaced laterally.

The above model is due to [23] who extended ideas of [10] on the creation of torques in anisotropic fluids by charge segregation. It provided a satisfactory explanation for the experimental observation of roll instabilities by [29,45]. Helfrich's dc model was extended to time-dependent fields by [17]. They found two different types of instability occurred at low and high frequencies. They called the former the conduction regime and the latter the dielectric regime with a critical frequency dividing them. The theory discussed thus far is one-dimensional and it was extended to two-dimensions by [39] who took account of the upper and lower boundaries. A review of this early work is given by [22]. The experimental work has also been developed by [26,42] to include multiple patterns and spatio-temporal chaos including defects. The onset of convection in the above models can be considered as a pitchfork bifurcation where the flow breaks the mid-plane symmetry and is analogous to Rayleigh–Bénard convection with a Boussinesq fluid. To date attempts to observe both branches of the pitchfork bifurcation experimentally have failed, see the papers by [25,38] where the side boundary conditions are different in each case. This is unlike the situation with Rayleigh–Bénard convection where the full bifurcation structure has been observed in small aspect ratio experiments by [1,44] as disconnected pitchforks. The experimental evidence suggests that the EHD case is more akin to the Taylor–Couette problem where the model bifurcation is drastically disconnected for both small aspect ratios, [2] and large aspect ratios [33]. Later extensions of the Carr—Helfrich model to include the flexo-electric effect, which removes this symmetry are reviewed by [31]. The preponderance of experimental studies consider the ac case to avoid the problems associated with charge injection at the electrodes. The injection of charges into weakly con-

ducting electrolytes can give rise to another form of cellular convection called the Felici instability [20]. In the problem studied by Felici, unipolar injection of charges at one of the electrodes can promote convection in direct analogy with the Rayleigh–Bénard problem, i.e. it does not involve space charge separation in anisotropic fluids which is essential for the Carr–Helfrich mechanism. Recent research by [25,34,41] report conflicting evidence for the importance of charge injection in EHD convection in a dc field. The finite-element calculations performed by [43] using the same technique as described here, reaffirm the importance of conductivity anisotropy in the Carr—Helfrich mechanism suggesting that the fundamental processes driving electrohydrodynamic convection in both the ac and dc cases are the same.

In Sections 2 and 3, we review the pertinent aspects of the continuum theory and those effects of an applied electric field that are relevant to electrohydrodynamic convection. We then describe our finite-element approach and the results from laboratory experiments and highlight the qualitatively similar features.

2. Continuum theory

We first review the essential continuum theory, concentrating on those aspects relevant to electrohydrodynamic convection. Throughout this section we use Cartesian tensor notation, double subscripts to denote summation and commas to indicate differentiation with respect to the relevant spatial variable. Thermal effects are ignored.

The continuum theory of Ericksen [18] and Leslie [32] for nematic liquid crystals assumes that the average molecular axis is described locally by a unit vector $\boldsymbol{n}$ and that the material is incompressible. That is, the constraints

$$\boldsymbol{n}_i \boldsymbol{n}_i = 1, \tag{1}$$

$$\boldsymbol{v}_{i,i} = 0, \tag{2}$$

apply, where $\boldsymbol{v}$ is the fluid velocity.

Balance laws representing conservation of linear and angular momentum are

$$\rho \dot{\boldsymbol{v}}_i = \rho \boldsymbol{F}_i + \boldsymbol{t}_{ij,j}, \tag{3}$$

$$\rho \boldsymbol{M}_i + e_{ijk}\boldsymbol{t}_{kj} + \boldsymbol{l}_{ij,j} = 0, \tag{4}$$

where $\boldsymbol{F}$ and $\boldsymbol{M}$ represent body forces and moments per unit mass, $\boldsymbol{t}$ and $\boldsymbol{l}$ are the stress and couple stress tensors, respectively, the superposed dot denotes the material time derivative and e_{ijk} is the alternator. The inertial term has been omitted from the second equation since it is generally considered negligible. The stress and couple stress tensors have the form

$$\boldsymbol{t}_{ij} = -p\,\delta_{ij} - \frac{\partial W}{\partial \boldsymbol{n}_{k,j}} \boldsymbol{n}_{k,i} + \tilde{\boldsymbol{t}}_{ij} \tag{5}$$

$$\boldsymbol{l}_{ij} = e_{ipq}\boldsymbol{n}_p \frac{\partial W}{\partial \boldsymbol{n}_{q,j}}, \tag{6}$$

where the pressure, p, arises from the constraint (2), W is the elastic energy density and $\tilde{\boldsymbol{t}}$ is the dynamic part of the stress tensor. The elastic energy density is assumed, following [21], to have the form

$$2W = K_1(\boldsymbol{n}_{i,i})^2 + K_2(\boldsymbol{n}_i e_{ijk}\boldsymbol{n}_{k,j})^2 + K_3 \boldsymbol{n}_{i,p}\boldsymbol{n}_p \boldsymbol{n}_{i,q}\boldsymbol{n}_q + (K_2 + K_4)(\boldsymbol{n}_{i,j}\boldsymbol{n}_{j,i} - (\boldsymbol{n}_{i,i})^2), \tag{7}$$

the K_i being constants. Following arguments proposed by [19], the elastic constants satisfy

$$K_1 > 0, \qquad K_2 > 0, \qquad K_3 > 0. \tag{8}$$

The dynamic part of the stress tensor is linear in the velocity gradients and has the form

$$\tilde{\boldsymbol{t}}_{ij} = \alpha_1 \boldsymbol{n}_p \boldsymbol{n}_k S_{pk} \boldsymbol{n}_i \boldsymbol{n}_j + \alpha_2 N_i \boldsymbol{n}_j + \alpha_3 N_j \boldsymbol{n}_i + \alpha_4 S_{ij} + \alpha_5 S_{ip}\boldsymbol{n}_p \boldsymbol{n}_j + \alpha_6 S_{jp}\boldsymbol{n}_p \boldsymbol{n}_i, \tag{9}$$

where

$$S_{ij} = \tfrac{1}{2}(\boldsymbol{v}_{i,j} + \boldsymbol{v}_{j,i}), \quad A_{ij} = \tfrac{1}{2}(\boldsymbol{v}_{i,j} - \boldsymbol{v}_{j,i}),$$
$$N_i = \dot{\boldsymbol{n}}_i - A_{ij}\boldsymbol{n}_j, \tag{10}$$

and the viscosity coefficients α_i are constants. Throughout we adopt the [36] relation, namely

$$\alpha_6 = \alpha_2 + \alpha_3 + \alpha_5. \tag{11}$$

The intrinsic viscous moment in (4) is then

$$e_{ijk}[\tilde{\boldsymbol{t}}_{ij}] = e_{ijk}\boldsymbol{n}_j \tilde{g}_k, \tag{12}$$

where $[\tilde{\boldsymbol{t}}]$ represents the skew-symmetric part of $\tilde{\boldsymbol{t}}$ and

$$\tilde{g}_i = (\alpha_2 - \alpha_3)N_i + (\alpha_5 - \alpha_6)S_{ij}\boldsymbol{n}_j. \tag{13}$$

Likewise, the body moment arising from the external electric field can be written in terms of a contribution associated with $\boldsymbol{n}$ and one has

$$\rho \boldsymbol{M} M_i = e_{ijk}\boldsymbol{n}_j G_k, \tag{14}$$

$$G_i = \varepsilon_0\, \Delta\varepsilon(\boldsymbol{E}_j \boldsymbol{n}_j)\boldsymbol{E}_i, \tag{15}$$

$$\Delta\varepsilon = \varepsilon_{\parallel} - \varepsilon_{\perp}, \tag{16}$$

where $\varepsilon_{\parallel}$ and $\varepsilon_{\perp}$ denote the dielectric susceptibilities of the material parallel and perpendicular to the director, respectively.

Using (12) and (14), the angular momentum equation becomes

$$\left(\frac{\partial W}{\partial \boldsymbol{n}_{i,j}}\right)_{,j} - \frac{\partial W}{\partial \boldsymbol{n}_i} + G_i + \tilde{g}_i + \gamma \boldsymbol{n}_i = 0, \tag{17}$$

the scalar γ being a Lagrange multiplier arising from the constraint (1). The balance of linear momentum equation becomes

$$\rho \dot{\boldsymbol{v}}_i = \rho \boldsymbol{F}_i - \tilde{p}_i + \tilde{h}_i + \tilde{\boldsymbol{t}}_{ij,j}, \tag{18}$$

with

$$\tilde{p} = p + W + \psi, \tag{19}$$

and

$$\tilde{h}_i = \tilde{g}_j \boldsymbol{n}_{j,i}, \tag{20}$$

where ψ denotes the energy associated with the electric field. Finally, to place restrictions on the viscosity coefficients, we use the entropy inequality

$$(\tilde{\boldsymbol{t}}_{ij}) S_{ij} - \tilde{g}_i N_i \geq 0, \tag{21}$$

where the round brackets indicate the symmetric part of the dynamic stress tensor $\tilde{\boldsymbol{t}}$.

Eqs. (17) and (18) together with (7), (9), (10), (13) and (15) are generally known as the Ericksen–Leslie equations and model flows of a nematic liquid crystals that are free of ions. However, these equations are insufficient to model electrohydrodynamic convection in nematics since ionic impurities are always present and the movement of ions in the sample comprises an essential part of the instability mechanism [16]. We therefore supplement the Ericksen–Leslie equations with Poisson's equation and the equation for conservation of charge. These are

$$\varepsilon_0 D_{i,i} = \rho_e \tag{22}$$

$$\frac{D\rho_e}{Dt} + j_{i,i} = 0 \tag{23}$$

respectively, where D is the electric displacement given by

$$D_i = \varepsilon_\perp \boldsymbol{E}_i + \Delta\varepsilon \boldsymbol{E}_j \boldsymbol{n}_j \boldsymbol{n}_i, \tag{24}$$

ρ_e is the charge density within the material and $\mathbf{j}$ the current density given by

$$j_i = \sigma_\perp \boldsymbol{E}_i + \Delta\sigma\, \boldsymbol{E}_j \boldsymbol{n}_j \boldsymbol{n}_i, \tag{25}$$

$$\Delta\sigma = \sigma_\parallel - \sigma_\perp. \tag{26}$$

The nematic's conductivities parallel and perpendicular to the director are given by $\sigma_\parallel$ and $\sigma_\perp$, respectively. For most nematic materials $\Delta\sigma$ is positive. Finally,

$$e_{ijk} \boldsymbol{E}_{k,j} = 0. \tag{27}$$

3. Electric fields

Based on experimental evidence that the initial instability is two-dimensional, it is reasonable to assume that the flow is two-dimensional and that the director, velocity and electric field vectors satisfy

$$\boldsymbol{n} = (\cos\theta, 0, \sin\theta), \qquad \boldsymbol{v} = (u, 0, v),$$
$$\boldsymbol{E} = (-\phi_{,x}, 0, -\phi_{,z}), \tag{28}$$

where θ, u, v and ϕ are all functions of x and z. The angle θ is the deflection of the director away from alignment with the plates and ϕ is the electric potential. Notice that the expressions for $\boldsymbol{n}$ and $\boldsymbol{E}$ automatically satisfy the constraints (1) and (27), while (2) implies

$$u_{,x} + \boldsymbol{v}_{,z} = 0. \tag{29}$$

The modified pressure, $\tilde{p}$, and the charge density, ρ_e, are also assumed to be functions of x and z alone.

Neglecting inertial terms, (see Berreman [4]), the balance of linear momentum equations is

$$-\rho_e \phi_{,x} - \tilde{p}_{,x} + \tilde{g}_i \boldsymbol{n}_{i,x} + \tilde{\boldsymbol{t}}_{xx,x} + \tilde{\boldsymbol{t}}_{xz,z} = 0, \tag{30}$$

$$-\rho_e \phi_{,z} - \tilde{p}_{,z} + \tilde{g}_i \boldsymbol{n}_{i,z} + \tilde{\boldsymbol{t}}_{zx,x} + \tilde{\boldsymbol{t}}_{zz,z} = 0, \tag{31}$$

where $\tilde{g}_x$, $\tilde{g}_z$, $\tilde{g}_i \boldsymbol{n}_{i,x}$, $\tilde{g}_i \boldsymbol{n}_{i,z}$ and $\tilde{\boldsymbol{t}}_{xx}$, $\tilde{\boldsymbol{t}}_{xz}$, $\tilde{\boldsymbol{t}}_{zx}$, $\tilde{\boldsymbol{t}}_{zz}$ are defined in Appendix A. In the above we have made extensive use of the Parodi relation (11) and we have also assumed that

$$\alpha_1 = 0. \tag{32}$$

This assumption gives some measure of simplification to the problem and is also justified in that α_1 has been found to be very small in most instances.

The y-component of the angular momentum Eq. (17) is zero and after elimination of the Lagrange multiplier γ between the x and z components we have

$$\begin{aligned} &-K(\theta_{,xx} + \theta_{,zz}) + \tilde{g}_x \sin\theta - \tilde{g}_z \cos\theta \\ &\quad + \varepsilon_0\, \delta\varepsilon(\phi_{,x}^2 \sin\theta\cos\theta - \phi_{,x}\phi_{,z}\cos 2\theta \\ &\quad - \phi_{,z}^2 \sin\theta\cos\theta) = 0, \end{aligned} \tag{33}$$

where (for simplicity of this exposition) we have made the assumption $K_1 = K_3 = K$.

Finally, Poisson's equation and the equation of conservation of charge are

$$\begin{aligned} &\rho_e + \varepsilon_0\varepsilon_\perp(\phi_{,xx} + \phi_{,zz}) + \varepsilon_0\, \delta\varepsilon((\phi_{,x}\cos\theta + \phi_{,z}\sin\theta)\cos\theta)_{,x} \\ &\quad + \varepsilon_0\, \delta\varepsilon((\phi_{,x}\cos\theta + \phi_{,z}\sin\theta)\sin\theta)_{,z} = 0, \end{aligned} \tag{34}$$

$$\begin{aligned} &u\rho_{e,x} + \boldsymbol{v}\rho_{e,z} - \sigma_\perp(\phi_{,xx} + \phi_{,zz}) \\ &\quad - \Delta\sigma((\phi_{,x}\cos\theta + \phi_{,z}\sin\theta)\cos\theta)_{,x} \\ &\quad - \Delta\sigma((\phi_{,x}\cos\theta + \phi_{,z}\sin\theta)\sin\theta)_{,z} = 0. \end{aligned} \tag{35}$$

In order to implement the finite-element method, the governing equations and boundary conditions were recast in weak form. The resulting weak equations are given in Appendix B.

Assuming a rectangular domain

$$A = \{(x, z) : -\boldsymbol{l}/2 \leq x \leq \boldsymbol{l}/2, -d/2 \leq z \leq d/2\},$$

the following nondimensional variables were introduced.

$$\begin{aligned} &\hat{x} = \frac{x}{\boldsymbol{l}}, \qquad \hat{z} = \frac{z}{d}, \qquad \hat{u} = \frac{\boldsymbol{l}}{k}u, \qquad \hat{\boldsymbol{v}} = \frac{\boldsymbol{l}^2}{dk}\boldsymbol{v}, \\ &\hat{\tilde{p}} = \frac{\boldsymbol{l}^2}{K}p, \qquad \hat{\rho}_e = \frac{d^2}{\varepsilon_0\varepsilon_\perp\phi_0}\rho_e, \qquad \hat{\phi} = \frac{1}{\phi_0}\phi, \end{aligned} \tag{36}$$

where $k = K/\alpha_2$, and the dimensionless parameters

$$\begin{aligned} &\lambda = \frac{\varepsilon_0\varepsilon_\perp\phi_0^2}{K}, \qquad r = \frac{\boldsymbol{l}}{d}, \qquad \mu = \frac{k\varepsilon_0\varepsilon_\perp}{\sigma_\perp d^2}, \\ &\varepsilon = \frac{\varepsilon_\parallel}{\varepsilon_\perp}, \qquad \sigma = \frac{\sigma_\parallel}{\sigma_\perp}, \end{aligned} \tag{37}$$

all of which are positive apart from μ, (for flow aligning, rod-like nematics $\alpha_2 < 0$).

Non-slip velocity boundary conditions and homogenous anchoring were enforced at the top and bottom plates, $\hat{z} = \pm 1/2$. The charge density ρ_e was required to be zero along conducting plates but not along insulating ones. Homeotropic anchoring of the director was applied on the lateral walls, $\hat{x} = \pm 1/2$ which were assumed to be perfectly insulating and stress-free. The electric potentials specified at the top and bottom plates were $\hat{\phi} = \pm 1/2$, respectively.

4. Numerical results

The weak form of the nondimensionalized equations were discretized and solved using the finite-element package Entwife [12]. All computations were performed using isoparametric quadrilateral elements with biquadratic interpolation for the velocity components $\hat{u}$ and $\hat{v}$, director angle θ, charge density $\hat{\rho}_e$ and electric potential $\hat{\phi}$. Discontinuous linear interpolation was used for the modified pressure field $\hat{\tilde{p}}$. A recent survey of the numerical techniques used here to compute bifurcation phenomena with particular application to the Navier–Stokes equations appears in [13]. A computer algebra package was used to write the subroutines needed to evaluate the derivatives required for the extended systems employed. A discussion of these implementation details appears in [14]. Tavener et al. [43] used these technqiues to investigate nonlinear interactions as for various aspect ratios, and studied the connection between electrohydrodynamic convection and the static Freedericksz transition as the conductivity anisotropy is varied.

Using the values of K, $\varepsilon_\perp$, α_2 and $\sigma_\perp$ for MBBA I listed in Appendix D of [8], we set

$$\mu = 0, \quad \varepsilon = 0.8, \quad \sigma = 1.5,$$

and

$$\alpha_2 = -0.1, \quad \alpha_3 = -0.0011,$$
$$\alpha_4 = 0.0826, \quad \alpha_5 = 0.0779.$$

When the electrical properties of the top and bottom plates are assumed to be different, the reflectional symmetry about the horizontal midplane is broken. The reflectional symmetry about the horizontal midplane was broken in the numerical calculations reported below by assuming that only the central section of the upper boundary was a conductor, generating a fringing electric field to model the finite size effects of the electrodes in the experiment. With these boundary conditions, flows with even numbers of cells (which respect the symmetry about the vertical midplane) develop continuously with quasistatic increase of the applied field, i.e. the symmetry-breaking pitchfork bifurcation of the perfect system is disconnected by the imperfection introduced by the fringing field. One of the two possible even-cell flows arises with continuous increase in applied electric field and

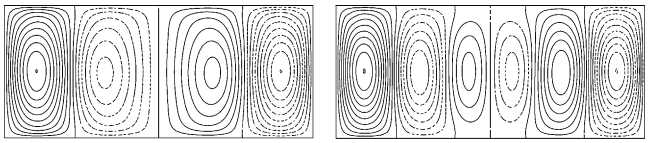

Fig. 3. Streamfunctions of the critical flows: (a) four-cell flow at $(\lambda, r) = (320, 2.335)$; (b) six-cell flow at $(\lambda, r) = (320, 2.325)$.

is termed the "primary flow". The other possible even-cell flow, (the mirror image of the "primary" flow) exists as a disconnected state above a critical value of the electric field. Streamfunctions of the four and six-cell flows involved in the exchange are shown at $\lambda = 320$ and aspect ratios $r \approx 2.335$ and $r \approx 2.325$ in Fig. 3. These flows correspond to the limit points at A and B, respectively in Fig. 4.

The limit point above which the disconnected state exists was determined in the following manner. At an aspect ratio of two, a four-cell flow is expected to develop with continuous increase in the applied electric field from zero, i.e. it is found as the primary flow. This branch of solutions was computed by performing arclength continuation [30] in λ, starting from a very small value of the electric field. At the fixed value of $\lambda = 350$, the aspect ratio was then increased until a limit point was detected at $\Gamma \approx 2.39$. At this value of the aspect ratio, continuous increase in the applied electric field leads to a six-cell "primary" flow and the four-cell is now secondary and terminated by a limit point. The path of limit points in the (λ, r)-plane was then calculated using the extended system technique developed by Moore and Spence [35] for both four and six cells.

The paths of limit points are shown in Fig. 4 and they have the characteristic cusp shape, which in this instance is aligned nearly parallel to the λ axis. For aspect ratios larger than the cusp point, the primary flow has six-cells, but four-cell flows also exist as a disconnected state for values of the electric field exceeding those corresponding to the upper line of limit points TA, shown in Fig. 4. For aspect ratios

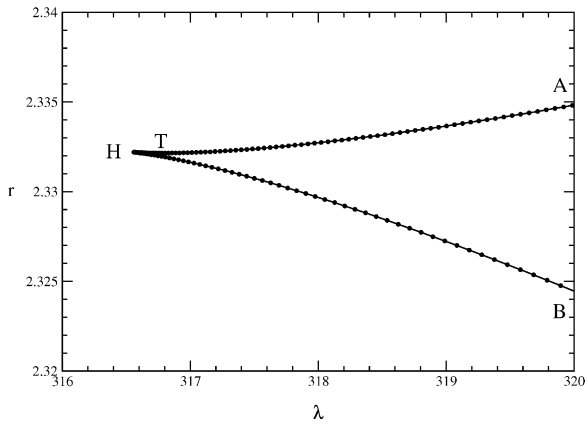

Fig. 4. Cusp mediating exchange between four-cell and six-cell flows for a small fringing field. ATCB is a path of limit points with a transcritical bifurcation point at T and a hysteresis point at H.

smaller than the cusp point, the primary flow is a four-cell flow, but a six-cell flow exists as a disconnected flow for values of the electric field exceeding those of the lower path of limit points, HB. The exchange of stabilities between the two disconnected states takes place at a transcritical bifurcation point which is not well resolved on the scale of Fig. 4. The cusp is located at $(\lambda, r) \approx (316.5, 2.3322)$ and the transcritical bifurcation point at $(\lambda, r) \approx (316.5, 2.3322)$. The sequence is qualitatively the same as the exchange of stabilities between $2n$ and $2(n+1)$-cell flows in the Taylor—Couette flow, first described by Benjamin [2].

We will discuss below an experimentally determined cusp from a nematic liquid crystal flow where the two parameters used to explore it are the voltage and frequency of the applied field.

5. Experiments

The liquid crystal cell used in all the experiments reported here comprised a $46 \pm 1.0\,\mu$m thick layer of the nematic liquid crystal BDH-17886 sandwiched between two optically flat glass plates. Indium-tin oxide line electrodes of width $\sim 185\,\mu$m were etched onto the inner surface of each plate. The electrodes were arranges so that they overlapped at right angles which created an active region of aspect ratio 4:4:1. Thus the entire cell was filled with nematic material but only a small square region was electrically active rather like a single pixcel on a computer display. The idea behind using such small aspect ratio devices is to limit the number of steady solutions so that individual interactions can be studied in detail.

The largest dimension of the active area was equivalent to only 10^5 molecular lengths and comparable to the width of a human hair, as illustrated in Fig. 5(a). On such a small scale inherent microscopic fluctuations are known to cause large variation in continuum quantities such as the director [16]. Alignment of the material, which was parallel to the lower electrode, was obtained using a rubbed layer of poly-vinyl alcohol (PVA) spin coated on top of the electrodes. The cell was mounted on a microscope translation stage and maintained at a constant temperature of $32.0 \pm 0.02\,^{\circ}$C. Applied ac voltages were of the order of $10\,V_{rms}$ and had a frequency of the order of 600 Hz. These parameters had a long term stability of better than 0.5%. The results are presented in terms of an nondimensionalised relative frequency $\boldsymbol{F}_n$ where a well defined bifurcation point was used as the calibration point. Details of this procedure can be found in [37]. Light transmitted through the cell was imaged using a CCD camera and the flow state was analysed using a computer imaging system.

An image of eight-cell flow is presented in Fig. 5(b). For $\boldsymbol{F}_n > 0.995$ this flow was primary [2,5], i.e. it smoothly evolved from the undisturbed field as the frequency was continuously reduced. In principle, the experiments could be performed by varying either the frequency or the voltage

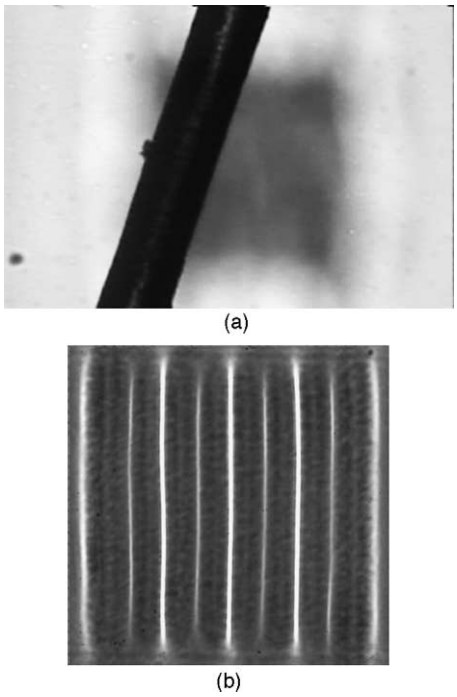

Fig. 5. (a) Image of the apparatus taken through a microscope with a human hair placed directly above the active area. The out of focus square shape beneath is made visible by the fluid motion inside the active region. (b) An eight-cell primary flow. Bright lines indicate upward convective flow and fainter lines indicate downward motion between a pair of counter-rotating convection cells.

while keeping the other fixed. In practice, we found it to be more convenient to perform the majority of the experiments by fixing voltages at prescribed values and then varying the frequency. At lower values of the frequency the primary flow comprised six convection cells. Clearly the respective

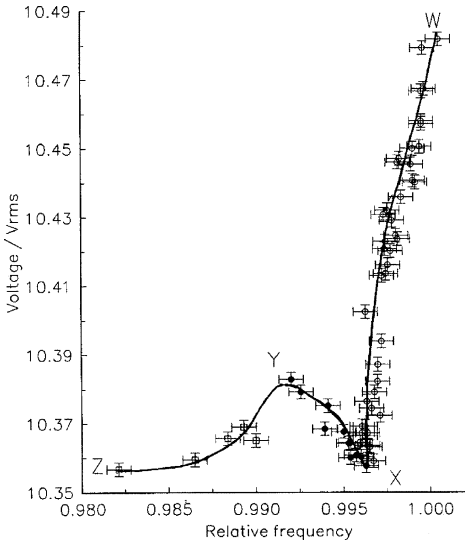

Fig. 6. Experimental bifurcation set. Empty circles and squares are estimates of the saddle nodes for the six and eight-cell modes, respectively. The filled circles are measures for the onset of six cells. (Data supplied by D.J. Binks)

primary states will be disconnected secondary modes in the neighbouring parameter ranges as discussed above. The loci of the critical points of the saddle nodes associated with the secondary modes were measured by observing the catastrophic loss of stability of the disconnected state as the frequency of the applied field was varied. These measured critical points have been used to construct Fig. 6. where the lines have been added to guide the eye. WX is the path of the six-cell secondary state and ZY that for the eight-cell. The path XY corresponds to the fold in the development of the six-cell flow and the transcritical bifurcation is near the location lablled Y in Fig. 6. This clearly identifiable feature and the fact that the experimental cusp is not aligned with either parameter axis suggests that the disconnection of the pitchfork in the experiment is far greater than that which is allowed by the fringing field model.

6. Conclusions

The qualitative nature of the primary flow exchange is the same in the experimental and numerical results. The control parameters available in the two systems are different as the experiment is driven by an ac field whereas a dc field is assumed in the numerical model. Nevertheless, the sequence of nonlinear events are clearly the same in each study. This demonstrates the robustness of Benjamin's hypothesis that the simplest way in which two smoothly developing cellular flows can exchange priority in a fluid flow is via a cusp and transcritical bifurcation. We have been able to confirm the details of the procedure in the Ericksen–Leslie equations using numerical bifurcation techniques and demonstrate that they are relevant to the physical system in our complimentary experimental study. The results demonstrate the power of our numerical methods which are capable of producing significant results in complex nonlinear flows on physically relevant boundary conditions.

Appendix A. Definitions

In Eqs. (30) and (31) the quantities $\tilde{g}_x$, $\tilde{g}_z$, $\tilde{g}_i \boldsymbol{n}_{i,x}$, $\tilde{g}_i \boldsymbol{n}_{i,z}$ are

$$\begin{aligned}\tilde{g}_x = {} & (\alpha_3 - \alpha_2) u \theta_{,x} \sin\theta + (\alpha_3 - \alpha_2) v \theta_{,z} \sin\theta \\ & - (\alpha_2 + \alpha_3) u_{,x} \cos\theta - \alpha_2 u_{,z} \sin\theta - \alpha_3 \boldsymbol{v}_{,x} \sin\theta,\end{aligned}$$

$$\begin{aligned}\tilde{g}_z = {} & (\alpha_2 - \alpha_3) u \theta_{,x} \cos\theta + (\alpha_2 - \alpha_3) v \theta_{,z} \cos\theta \\ & - (\alpha_2 + \alpha_3) \boldsymbol{v}_{,z} \sin\theta - \alpha_3 u_{,z} \cos\theta - \alpha_2 \boldsymbol{v}_{,x} \cos\theta,\end{aligned}$$

$$\begin{aligned}\tilde{g}_i \boldsymbol{n}_{i,x} = {} & (\alpha_2 - \alpha_3) u \theta_{,x}^2 \sin^2\theta + (\alpha_2 - \alpha_3) v \theta_{,x} \theta_{,z} \sin^2\theta \\ & + (\alpha_2 + \alpha_3) u_{,x} \theta_{,x} \sin\theta \cos\theta + \alpha_2 u_{,z} \theta_{,x} \sin^2\theta \\ & + \alpha_3 \boldsymbol{v}_{,x} \theta_{,x} \sin^2\theta + (\alpha_2 - \alpha_3) u \theta_{,x}^2 \cos^2\theta \\ & + (\alpha_2 - \alpha_3) v \theta_{,x} \theta_{,z} \cos^2\theta \\ & - (\alpha_2 + \alpha_3) \boldsymbol{v}_{,z} \theta_{,x} \sin\theta \cos\theta \\ & - \alpha_3 u_{,z} \theta_{,x} \cos^2\theta - \alpha_2 \boldsymbol{v}_{,x} \theta_{,x} \cos^2\theta,\end{aligned}$$

$$\begin{aligned}\tilde{g}_i \boldsymbol{n}_{i,z} = {} & (\alpha_2 - \alpha_3) u \theta_{,x} \theta_{,z} \sin^2\theta + (\alpha_2 - \alpha_3) v \theta_{,z}^2 \sin^2\theta \\ & + (\alpha_2 + \alpha_3) u_{,x} \theta_{,z} \sin\theta \cos\theta + \alpha_2 u_{,z} \theta_{,z} \sin^2\theta \\ & + \alpha_3 \boldsymbol{v}_{,x} \theta_{,z} \sin^2\theta + (\alpha_2 - \alpha_3) u \theta_{,x} \theta_{,z} \cos^2\theta \\ & + (\alpha_2 - \alpha_3) v \theta_{,z}^2 \cos^2\theta - (\alpha_2 + \alpha_3) \boldsymbol{v}_{,z} \theta_{,z} \sin\theta \cos\theta \\ & - \alpha_3 u_{,z} \theta_{,z} \cos^2\theta - \alpha_2 \boldsymbol{v}_{,x} \theta_{,z} \sin\theta \cos\theta,\end{aligned}$$

In Eqs. (30) and (31) the components of the stress tensor $\tilde{\boldsymbol{t}}_{xx}$, $\tilde{\boldsymbol{t}}_{xz}$, $\tilde{\boldsymbol{t}}_{zx}$, $\tilde{\boldsymbol{t}}_{zz}$ are

$$\begin{aligned}\tilde{\boldsymbol{t}}_{xx} = {} & (\alpha_4 + (\alpha_2 + \alpha_3 + 2\alpha_5)\cos^2\theta) u_{,x} \\ & + \alpha_5 u_{,z} \sin\theta \cos\theta + (\alpha_2 + \alpha_3 + \alpha_5) \boldsymbol{v}_{,x} \sin\theta \cos\theta \\ & - (\alpha_2 + \alpha_3) u \theta_{,x} \sin\theta \cos\theta - (\alpha_2 + \alpha_3) v \theta_{,z} \sin\theta \cos\theta,\end{aligned}$$

$$\begin{aligned}\tilde{\boldsymbol{t}}_{xz} = {} & (\alpha_3 \cos^2\theta - \alpha_2 \sin^2\theta) u \theta_{,x} + (\alpha_3 \cos^2\theta - \alpha_2 \sin^2\theta) v \theta_{,z} \\ & + \tfrac{1}{2}(\alpha_2 + \alpha_4 + \alpha_5 + 2(\alpha_3 \cos^2\theta - \alpha_2 \sin^2\theta)) u_{,z} \\ & + \tfrac{1}{2}(\alpha_2 + \alpha_4 + \alpha_5) \boldsymbol{v}_{,x} + \alpha_5 u_{,x} \sin\theta \cos\theta \\ & + (\alpha_2 + \alpha_3 + \alpha_5) \boldsymbol{v}_{,z} \sin\theta \cos\theta,\end{aligned}$$

$$\begin{aligned}\tilde{\boldsymbol{t}}_{zx} = {} & (\alpha_2 - \alpha_3 + \alpha_3 \cos^2\theta - \alpha_2 \sin^2\theta) u \theta_{,x} \\ & + (\alpha_2 - \alpha_3 + \alpha_3 \cos^2\theta - \alpha_2 \sin^2\theta) v \theta_{,z} \\ & + \tfrac{1}{2}(\alpha_2 + \alpha_4 + \alpha_5) u_{,z} + \tfrac{1}{2}(-\alpha_2 + 2\alpha_3 + \alpha_4 + \alpha_5 \\ & - 2(\alpha_3 \cos^2\theta - \alpha_2 \sin^2\theta)) \boldsymbol{v}_{,x} + \alpha_5 \boldsymbol{v}_{,z} \sin\theta \cos\theta \\ & + (\alpha_2 + \alpha_3 + \alpha_5) u_{,x} \sin\theta \cos\theta,\end{aligned}$$

$$\begin{aligned}\tilde{\boldsymbol{t}}_{zz} = {} & (\alpha_2 + \alpha_3) u \theta_{,x} \sin\theta \cos\theta \\ & + (\alpha_2 + \alpha_3) v \theta_{,z} \sin\theta \cos\theta \\ & + (\alpha_2 + \alpha_3 + \alpha_5) u_{,z} \sin\theta \cos\theta + \alpha_5 \boldsymbol{v}_{,x} \sin\theta \cos\theta \\ & + (\alpha_4 + (\alpha_2 + \alpha_3 + 2\alpha_5) \sin^2\theta) \boldsymbol{v}_{,z}.\end{aligned}$$

Appendix B. Weak form of the equilibrium equations

The weak form of Eqs. (29), (30), (31), (33), (34) and (35) are

$$\int_A (u_{,x} + \boldsymbol{v}_{,z}) w_1 \, \mathrm{d}x \, \mathrm{d}z = 0 \tag{B.1}$$

$$\begin{aligned}& \int_S (-\tilde{p} + \tilde{\boldsymbol{t}}_{xx}) w_2 \, \mathrm{d}z - \int_S \tilde{\boldsymbol{t}}_{xz} w_2 \, \mathrm{d}x \\ & + \int_A (-\rho_e \phi_{,x} + \tilde{g}_i \boldsymbol{n}_{i,x}) w_2 \, \mathrm{d}x \, \mathrm{d}z \\ & - \int_A (-\tilde{p} + \tilde{\boldsymbol{t}}_{xx}) w_{2,x} \, \mathrm{d}x \, \mathrm{d}z - \int_A \tilde{\boldsymbol{t}}_{xz} w_{2,z} \, \mathrm{d}x \, \mathrm{d}z = 0\end{aligned} \tag{B.2}$$

$$\int_S \tilde{\boldsymbol{t}}_{zx} w_3 \,\mathrm{d}z - \int_S (-\tilde{p} + \tilde{\boldsymbol{t}}_{zz}) w_3 \,\mathrm{d}x + \int_A (-\rho_e \phi_{,z} + \tilde{g}_i \boldsymbol{n}_{i,z}) w_3 \,\mathrm{d}x\,\mathrm{d}z - \int_A \tilde{\boldsymbol{t}}_{zx} w_{3,x} \,\mathrm{d}x\,\mathrm{d}z - \int_A (-\tilde{p} + \tilde{\boldsymbol{t}}_{zz}) w_{3,z} \,\mathrm{d}x\,\mathrm{d}z = 0 \quad \text{(B.3)}$$

$$-\int_S K\theta_{,x} w_4 \,\mathrm{d}z + \int_S K\theta_{,z} w_4 \,\mathrm{d}x + \int_A (\tilde{g}_x \sin\theta - \tilde{g}_z \cos\theta + \varepsilon_0 \,\delta\varepsilon(\phi_{,x}^2 \sin\theta\cos\theta - \phi_{,x}\phi_{,z} \cos 2\theta - \phi_{,z}^2 \sin\theta\cos\theta)) w_4 \,\mathrm{d}x\,\mathrm{d}z + \int_A K\theta_{,x} w_{4,x} \,\mathrm{d}x\,\mathrm{d}z + \int_A K\theta_{,z} w_{4,z} \,\mathrm{d}x\,\mathrm{d}z = 0 \quad \text{(B.4)}$$

$$\int_S \varepsilon_0(\varepsilon_\perp \phi_{,x} + \Delta\varepsilon(\phi_{,x}\cos\theta + \phi_{,z}\sin\theta)\cos\theta) w_5 \,\mathrm{d}z - \int_S \varepsilon_0(\varepsilon_\perp \phi_{,z} + \Delta\varepsilon(\phi_{,x}\cos\theta + \phi_{,z}\sin\theta)\sin\theta) w_5 \,\mathrm{d}x + \int_A \rho_e w_5 \,\mathrm{d}x\,\mathrm{d}z - \int_A \varepsilon_0(\varepsilon_\perp \phi_{,x} + \Delta\varepsilon(\phi_{,x}\cos\theta + \phi_{,z}\sin\theta)\cos\theta) w_{5,x} \,\mathrm{d}x\,\mathrm{d}z - \int_A \varepsilon_0(\varepsilon_\perp \phi_{,z} + \Delta\varepsilon(\phi_{,x}\cos\theta + \phi_{,z}\sin\theta)\sin\theta) w_{5,x} \,\mathrm{d}x\,\mathrm{d}z = 0 \quad \text{(B.5)}$$

$$-\int_S (\sigma_\perp \phi_{,x} + \Delta\sigma(\phi_{,x}\cos\theta + \phi_{,z}\sin\theta)\cos\theta) w_6 \,\mathrm{d}z + \int_S (\sigma_\perp \phi_{,z} + \Delta\sigma(\phi_{,x}\cos\theta + \phi_{,z}\sin\theta)\sin\theta) w_6 \,\mathrm{d}x + \int_A (u\rho_{e,x} + v\rho_{e,z}) w_6 \,\mathrm{d}x\,\mathrm{d}z + int_S(\sigma_\perp \phi_{,x} + \Delta\sigma(\phi_{,x}\cos\theta + \phi_{,z}\sin\theta)\cos\theta) w_{6,x} \,\mathrm{d}x\,\mathrm{d}z + \int_A (\sigma_\perp \phi_{,x} + \Delta\sigma(\phi_{,z}\cos\theta + \phi_{,z}\sin\theta)\sin\theta) w_{6,x} \,\mathrm{d}x\,\mathrm{d}z = 0 \quad \text{(B.6)}$$

References

[1] M.P. Arroyo, J.M. Saviron, Rayleigh–Bénard convection in a small box-spatial features and thermal-dependence of the velocity-field, J. Fluid Mech. 235 (1992) 325–348.

[2] T.B. Benjamin, Bifurcation phenomena in steady flows of a viscous fluid, Proc. Roy. Soc. Lond. A 359 (1978) 1–43.

[3] D.W. Berreman, Solid surface shape and the alignment of an adjacent nematic liquid crystal, Phys. Rev. Lett. 28 (1972) 1683–1686.

[4] D.W. Berreman, Liquid-crystal twist cell dynamics with backflow, J. Appl. Phys. 46 (1975) 3746–3751.

[5] D.J. Binks, T.Mullin, Cell number selection in electrohydrodynamic convection in liquid crystals, Proc. R. Soc. Lond. A 453 (1997) 2109–2122.

[6] G.I. Blake, S.J. Tavener, T.Mullin, The Freedericksz transition as a bifurcation problem, Dynam. Stab. Syst. 14 (1999) 299–331.

[7] L.M. Blinov, Electro-optical and Magneto-optical Properties of Liquid Crystals, Wiley, 1983.

[8] E.Bodenschatz, W.Zimmermann, L.Kramer, On electrically driven pattern-forming instabilities in planar nematics, J. Phys. France 453 (1988) 1875–1899.

[9] A.Buka, L.Kramer, Pattern Formation in Liquid Crystals, Springer, 1996.

[10] E.F. Carr, Influence of an electric field on the dielectric loss of of the liquid-crystal *p*-azoxyanisole, J. Chem. Phys. 39 (1963) 1979–1983.

[11] S.Chandrasekhar, Liquid Crystals, Cambridge University Press, 1977.

[12] K.A. Cliffe, Entwife (release 6.3) reference manual: entwife, initial data and solver data commands, AEAT-0823, 1996.

[13] K.A. Cliffe, A. Spence, S.J. Tavener, The Numerical Analysis of Bifurcation Problems with Application to Fluid Mechanics, Acta Numerical, 2000, pp. 39–131.

[14] K.A. Cliffe, S.J. Tavener, Implementation of extended systems using symbolic algebra, In: D. Henry, A. Bergeon (Eds.), Continuation Methods in Fluid Dynamics, Notes on Numerical Fluid Mechanics, 2000, pp. 81–92.

[15] M.C. Cross, P.C. Hohenberg, Pattern formation outside equilibrium, Rev. Mod. Phys. 65 (1993) 851–1112.

[16] P.G. de Gennes, J. Prost, The Physics of Liquid Crystals, Oxford University Press, 1993.

[17] E. Dubois-Violette, P.G. de Gennes, O. Parodi, Hydrodynamic instabilities of nematic liquid crystals under ac electric fields, J. Phys. Paris 32 (1973) 305–317.

[18] J.L. Ericksen, Hydrostatic theory of liquid crystals, Arch. Rat. Mech. Anal. 9 (1962) 371.

[19] J.L. Ericksen, Inequalities in liquid crystal theory, Phys. Fluids 9 (1966) 1205–1207.

[20] N. Felici, Phénoménes hydro et aérodynamiques dans la conduction des diélectriques fluides, Rev. Gén. de L'Élect. 78 (1969) 717–734.

[21] F.C. Frank, On the theory of liquid crystals, Discuss. Faraday Soc. 25 (1958) 19–28.

[22] W.J.A. Goossens, Electrohydrodynamic instabilities in nematic liquid crystals, Adv. Liq. Cryst. 3 (1978) 1–38.

[23] W. Helfrich, Conduction-induced alignment of nematic liquid crystals: basic model and stability considerations, J. Chem. Phys. 51 (1969) 4092–4105.

[24] Y. Hidaka, K. Shimokawa, H. Orihara, T. Nagaya, Y. Ishibashi, Evolution processes of the Williams domain in electrohydrodynamic systems with free and rigid lateral boundaries, J. Phys. Soc. Jpn. 63 (1994) 1698–1712.

[25] S. Hirata, T. Tako, Effect of cell width on the structure of Williams domain, Jpn. J. App. Phys. 21 (1982) L607–L609.

[26] A. Joets, R. Ribotta, Hydrodynamic transitions to chaos in convection of an isotropic fluid, J. Physique 47 (1986) 595–606.

[27] S. Kai, K. Hirakawa, Successive transitions in electrohydrodynamic instabilities of nematics, Prog. Theor. Phys. Suppl. 64 (1978) 212–243.

[28] S. Kai, W. Zimmermann, Pattern dynamics in the electrohydrodynamics of nematic liquid crystals, Prog. Theor. Phys. Suppl. 99 (1989) 458–492.

[29] A.P. Kasputin, L.S. Larionova, On the behaviour of anisotropic liquids in electric fields, Sov. Phys. Cryst. 9 (1964) 297–300.

[30] H.B. Keller, Numerical solution of bifurcation and nonlinear eigenvalue problems, in: P. Rabinowitz (Ed.), Applications of Bifurcations Theory, Academic Press, NY, 1977, pp. 359–384.

[31] L.Kramer, W.Pesch, Convection instabilities in nematic liquid crystals, Ann. Rev. Fluid Mech. 27 (1995) 515–541.

[32] F.M. Leslie, Continuum theory for nematic liquid crystals, Continuum Mech. Thermodyn. 4, 1992.

[33] A. Lorenzen, T. Mullin, End effects and anomalous modes in Taylor–Couette flow, Phys. Rev. A 31 (1985) 3463–3465.
[34] N.V. Madhusudana, V.A. Raghunathan, K.R. Sumathy, Electrohydrodynamic instabilities in nematic liquid crystals in low-frequency fields, Pramana J. Phys. 28 (1987) L311–L316.
[35] G. Moore, A. Spence, The calculation of turning points of nonlinear equations, SIAM J. Num. Anal. 17 (1980) 567–576.
[36] O. Parodi, Stress tensor for a nematic liquid crystal, J. Phys. 31 (1970) 581–584.
[37] T. Peacock, D.J. Binks, T. Mullin, From low- to high-dimensional dynamics in a microscopic fluid flow, Phys. Rev. Lett. 82 (1999) 1446–1449.
[38] T. Peacock, T. Mullin, D.J. Binks, Bifurcation phenomena in flows of a nematic liquid crystal, Int. J. Bif. Chaos 9 (1999) 427–441.
[39] P.A. Penz, Electrohydrodynamic solutions for nematic liquid crystals with positive dielectric anisotropy, Mol. Cryst. Liq. Cryst. 23 (1973) 1–11.
[40] W. Pesch, U. Behn, Electrohydrodynamic convection in nematics, in: F.H. Busse, S.C. Mueller (Eds.), Evolution of Spontaneous Structures in Dissipative Continuous Systems, Springer, 1998, pp. 335–383.
[41] V.A. Raghunathan, N.V. Madhusudana, Flexoelectric origin of oblique rolls with helical flow in electroconvective nematics under dc excitation, Pramana J. Phys. 31 (1988) L163–L167.
[42] I. Rehberg, S. Rasenat, V. Steinberg, Traveling waves and defect-initiated turbulence in electroconvecting nematics, Phys. Rev. Lett. 62 (1989) 756–759.
[43] S.J. Tavener, G.I. Blake, T. Mullin, K.A. Cliffe, A numerical bifurcation study of electrohydrodynamic convection in nematic liquid crystals, Phys. Rev. E 63 (2001) 011708.
[44] P.A. Warkentkin, H.J. Haucke, P. Lucas, J.C. Wheatley, Stationary convection in dilute solutions of ^{3}He in superfluid ^{4}He, Proc. Natl. Acad. Sci. U.S.A. 77 (1980) 6983–6987.
[45] R. Williams, Domains in liquid crystals, J. Chem. Phys. 39 (1963) 384–389.